Turkish Journal of Electrical Engineering & Computer Sciences

http://journals.tubitak.gov.tr/elektrik/

Research Article

Turk J Elec Eng & Comp Sci
(2013) 21: 1820 – 1826

doi:10.3906/elk-1201-6

# An improved back projection imaging algorithm for subsurface target detection

**Wentai LEI,**[1,*] **Sheng ZENG,**[2] **Jian ZHAO,**[2] **Qianzhe WANG,**[3] **Jianxin LIU**[4]

[1]School of Information Science and Engineering, Central South University, Changsha, China
[2]Institute of Traffic Science, Changsha University of Science and Technology, Changsha, China
[3]Department of Scientific Research, Air Force Engineering University, Xi'an, China
[4]School of Geosciences and Info-physics, Central South University, Changsha, China

**Received:** 04.01.2012 • **Accepted:** 14.05.2012 • **Published Online:** 02.10.2013 • **Printed:** 28.10.2013

**Abstract:** An improved back projection imaging algorithm for subsurface target detection is presented in this paper. Firstly, the characteristic of the scattering data at each time-delay curve in the traditional back projection imaging procedure is analyzed. Secondly, a weight factor is designed for each focal point and an improved back projection imaging algorithm is presented. Thirdly, the simulation of the improved imaging algorithm is processed. The imaging results of both the simulation data and the real ground penetrating radar data show the effectiveness of this imaging algorithm.

**Key words:** Back projection, radar imaging, ground penetrating radar, improved imaging algorithm

## 1. Introduction

Wide-band radar has been widely used in subsurface remote-sensing applications [1,2]. The application of ground penetrating radar (GPR) in the detection and discrimination of small objects, such as shallow buried landmines and unexploded ordnances, is currently receiving much attention [2,3]. Compared with other methods, radar imaging technology is the most efficient and direct one in target detection and recognition when coupled with the synthetic aperture technique [4].

Based on the 'delay and sum' operation, the traditional GPR back projection (BP) algorithm is suitable for subsurface imaging under conditions such as lossy layer media [4]. Gu et al. analyzed the BP imaging mechanism and provided the relevant equation. This algorithm is successfully used in forward-looking GPR data processing. However, the imaging results show a much higher side lobe and cannot meet the need of high-resolution purpose. Based on basic electromagnetic radiation theory, Lei et al. analyzed the GPR wave's radiation characteristic in subsurface layered medium and provided the corresponding BP imaging algorithm. It can also be shown that the BP imaging algorithm can preserve the object's electromagnetic resonance signal to the succeeding object's recognition [5]. However, the high side lobe characteristic limits its scope of application. Zhou et al. proposed a novel artifact suppression technique and provided a BP imaging algorithm based on cross correlation [6]. However, the information included in the one-dimensional (1-D) data located at the time-delay curve was not used sufficiently, and so the imaging quality is not as good.

To improve the quality of the GPR imaging results, an improved BP imaging algorithm is studied in this paper. This paper is organized as follows. In Section 2, the characteristic of the scattering data at each time-

*Correspondence: leiwentai@163.com

delay curve is analyzed, and then a weight factor is designed for each focal point and an improved BP imaging algorithm is presented. In Section 3, the simulation experiments and real-data experiment of the improved BP imaging algorithm are processed. The imaging results of the multitargets are presented and contrasted with the traditional BP imaging results.

## 2. Improved BP algorithm

The scene of a monostatic GPR measurement setup is shown in Figure 1. An impulse signal is transmitted by the GPR antenna to illuminate a subsurface area. The antenna is positioned at $(-r_a, -h_a)$ and it synthesizes an aperture on a line parallel to the $X$ axis at a distance $h_a$. The main lobe width of the antenna is $2\beta$ and the synthesized aperture length of the objects located at a depth of $h_b$ is $2(r_a + r_b)$. As the transmitter/receiver (T/R) antenna pair move along the aperture line $z = -h_a$ with the interval of $\Delta x$, multiscattering signals $e_1(x,t)$ at each focal aperture point $x_p = -r_a + (p-1)\Delta x, p = 1, \cdots, P$ can be obtained. Thus, the total scan number is $P = 1 + \frac{2(r_a+r_b)}{\Delta x}$. The purpose of the GPR imaging is to convert $e_1(x,t)$ to $e_2(x,z)$, that is to say, by the process $e_1(x,t)$ profile, the scattering density profile of the scanning region can be obtained.

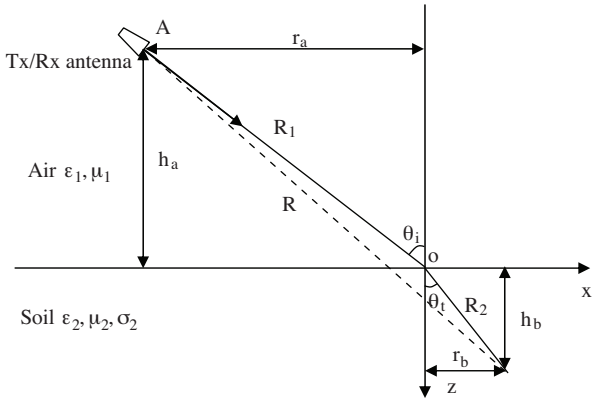


**Figure 1.** Scenario of the monostatic GPR detection.

The traditional BP imaging algorithm is a basic and well-known method [4,5]. The idea of this imaging algorithm is to sum all of the data coherently at one focal point $(x_n, z_m)$ in the ground at a time and repeat for all of the points in the range of interest (ROI). During the imaging, the focal point moves from one position to another within the whole ROI. At each position, all of the time-shifted responses are coherently summed and integrated. The relevant equation is:

$$e_2(x_n, z_m) = \sum_{p=1}^{P} e_1'(x_p, \tau_{m,n,p}), \tag{1}$$

where $e_1'(x,t)$ is the radar-gram after the preprocessing procedure, and $\tau_{m,n,p}$ is the travel time from the transmitter to the focal point and back to the receiver:

$$\tau_{m,n,p} = \frac{2R_a}{c} + \frac{2R_b}{v}, \tag{2}$$

where $c$ and $v$ are the propagation velocities in the air and soil, respectively, and $R_a$ and $R_b$ are the distances from the refraction points on the ground surface to the T/R pair point $(x_p, z = -h_a)$ and focal point $(x_n, z_m)$,

respectively. The main advantage of the BP imaging algorithm is its simplicity and suitability for parallel computing, but it is limited by its side lobe quality and imaging resolution.

In fact, more information can be obtained from the original radar-gram $e_1(x,t)$. At such points $(x_n, z_m)$ where there are real targets, the scattering data on the time-delay curve $e_1(x_p, t=\tau_{m,n,p})$ has distinctive statistic features. The 1-D data has good correlation. The ratio of the mean value and the standard deviation of $e_1(x_p, t=\tau_{m,n,p})$ is much bigger than the corresponding value of the other points where there are no real targets. Thus, this characteristic can be used to modify the traditional BP imaging algorithm.

By designing a new additional weighting factor $w(x_n, z_m)$, the imaging quality can be improved significantly. The weighting factor $w$ can be interpreted as a mask to the traditional BP imaging results. Using the statistic features, the weighting factor can subsequently be designed. It can be calculated in 3 steps. First, for each focal point, the scattering data $e_1'(x_p, t=\tau_{m,n,p})$ at the time-delay curve need to be extracted from the original radar-gram. Next, the mean value and standard deviation are calculated as shown below:

$$m = \frac{\sum_{p=1}^{P} e_1'(x_p, t=\tau_{m,n,p})}{P}, \tag{3}$$

$$v = \left\{ \frac{1}{P} \sum_{p=1}^{P} \left[ e_1'(x_p, t=\tau_{m,n,p}) - m \right]^2 \right\}^{\frac{1}{2}}. \tag{4}$$

In the third step, the weighting factor $w(x_n, z_m)$ is calculated as:

$$w(x_n, z_m) = \begin{cases} 1, & v = 0 \\ \frac{m}{v}, & otherwise \end{cases}. \tag{5}$$

Thus, the improved BP imaging algorithm can be expressed as:

$$e_3(x_n, z_m) = w(x_n, z_m) \sum_{p=1}^{P} e_1'(x_p, \tau_{m,n,p}). \tag{6}$$

In the following section, the experimental results of the improved BP imaging algorithm will be presented.

## 3. Simulation experiments and imaging results

In this section, we apply the improved BP imaging algorithm to some simulation data and real GPR data. The simulation data are obtained using the finite difference time domain (FDTD) method [7].

### 3.1. Case 1: Simulation data experiments

**Example 1.** Four metal bars are located at the points (0.7,0.7), (0.9,0.7), (1.2,0.7), and (1.6,0.7), respectively. Figure 2a shows the original GPR detection scenario of the multitargets. The relative permittivity of the background medium is 16. The T/R antenna pair is moved from the point (0.2,0) to the point (1.8,0), with the interval space of 0.02 m. Thus, the total aperture number is 81. At each aperture point, the transmitting antenna is excited by a Ricker wavelet whose center frequency is 400 MHz and the scattering signal is received by the receiving antenna. Each A-scan contains 4240 sampling points in the total 40 ns time window. After

finishing the scan procedure along the aperture line, a B-scan profile of the scanning region can be obtained. Before the imaging processing, a preprocessing procedure such as direct wave subtracting or inverse filtering is needed [1]. Figure 2b shows the B-scan profile after preprocessing. The traditional and improved BP imaging results are shown in Figures 2c and 2d, respectively.

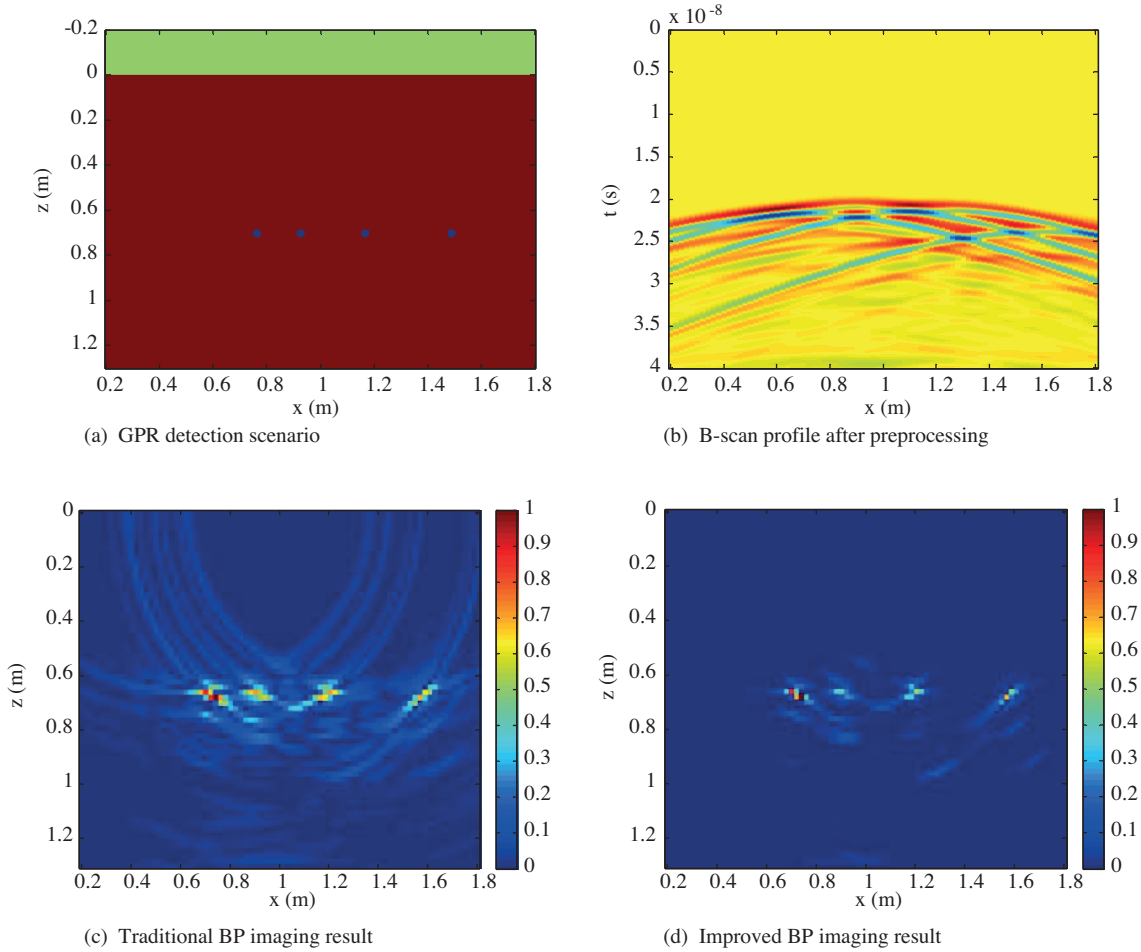


**Figure 2.** Multitarget simulation results in Example 1.

By contrasting the 2 imaging results, it is obvious that the improved BP imaging algorithm can obtain a better imaging result. The latter result shows a lower side lobe level and higher focusing quality. In order to quantitatively assess the imaging results, a focusing parameter is used here [8]. The focusing parameter of a 2-D imaging result $O(x,z)$ can be calculated as below:

$$f_O = \frac{\sum_{x=x_1}^{x_n}\sum_{z=z_1}^{z_m}\left[O(x_n,z_m)\right]^4}{\left\{\sum_{x=x_1}^{x_n}\sum_{z=z_1}^{z_m}\left[O(x_n,z_m)\right]^2\right\}^2}. \tag{7}$$

The focusing parameters of the above 2 imaging results are 0.00854 and 0.0578, respectively. The focusing quality of the imaging result improved by nearly 580%. On a PC platform with a 2.0-GHz CPU and 2.0-GB RAM, the time consumption of the 2 algorithms is 12.3 s and 14.3 s, respectively.

**Example 2.** Five metal bars are located at the points (0.7,0.7), (1.0,0.7), (1.3,0.7), (0.85,0.5), and (1.15,0.5), respectively. Figure 3a shows the original GPR detection scenario of the multitargets. The simulation parameters are the same as the above example. Figure 3b shows the B-scan profile after the preprocessing. The traditional and improved BP imaging results are shown in Figures 3c and 3d, respectively. Using the evaluation method of the focusing parameter as shown in Eq. (7), the focusing quality of the imaging results improved by nearly 690%. The time consumption of the improved BP algorithm increased by about 15%.

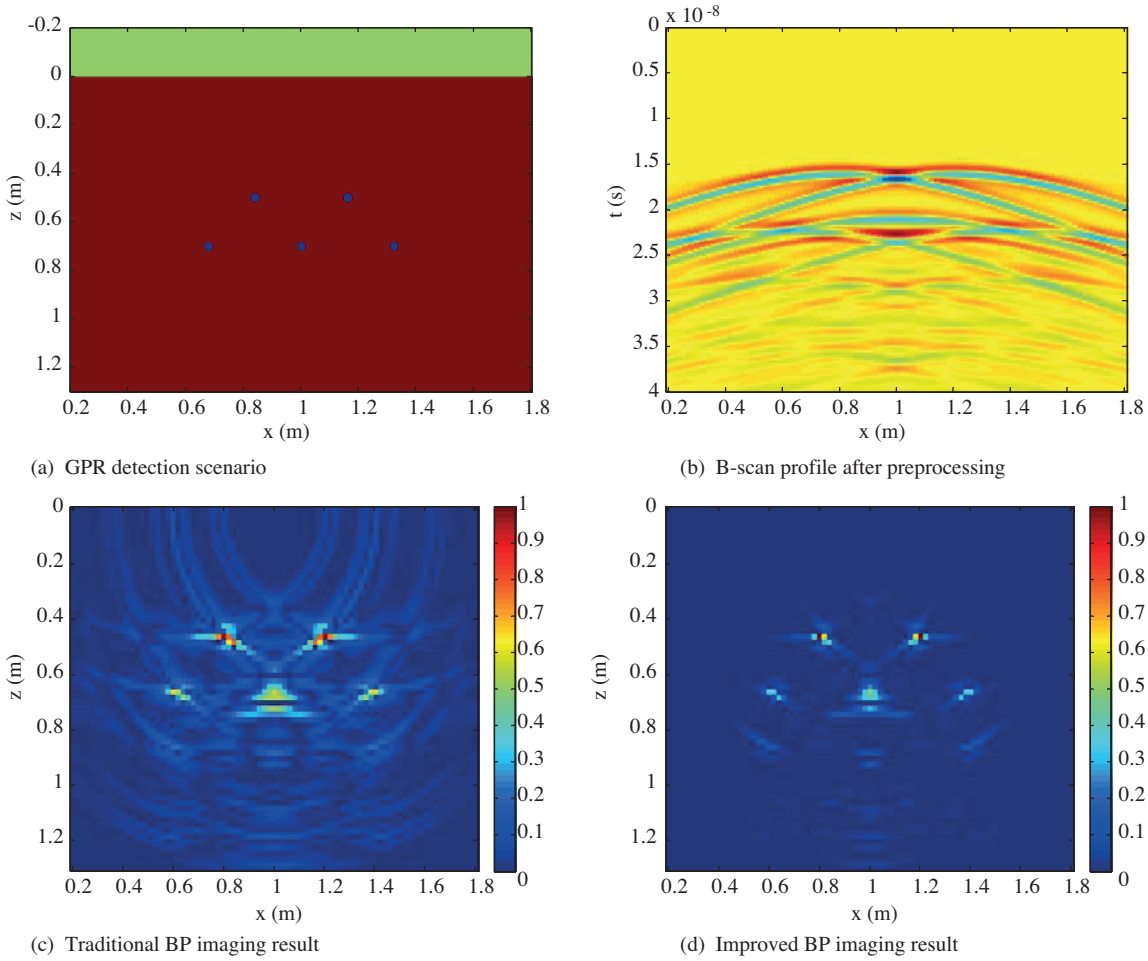


**Figure 3.** Multitarget simulation results in Example 2.

### 3.2. Case 2: Measured data experiment

A GPR survey was conducted along a provincial road in Hunan Province to investigate the practicality of the method for imaging the subsurface targets for a road quality assessment. A site across a subsurface culvert was chosen. The culvert has a width of 2 m and the thickness between its top point and the road surface is 1.3 m. In the first layer of the on-site road, the steel reinforcement is embedded in the protective concrete. We use an impulse GPR system equipped with a 400 MHz antenna pair to detect the abnormal subsurface. The B-scan line is selected along the road and has a length of 10.5 m.

The original data are shown in Figure 4a. After the preprocessing, we use the traditional and the improved BP imaging algorithms to obtain 2-D subsurface imaging results. The 2 imaging results are shown in Figures

4b and 4c, respectively. From the original GPR data and the imaging results, the steel reinforcement and the top surface of the subsurface culvert can be recognized clearly. In contrast with the traditional BP imaging algorithm, the time consumption of the improved BP imaging algorithm increased by about 5% and its focusing quality of the imaging results improved by nearly 10%. To show the contrast of the imaging results clearly, the imaging results of the steel reinforcement region are displayed separately, as shown in Figure 4d. The focusing quality of this section's imaging results improved by nearly 20%.

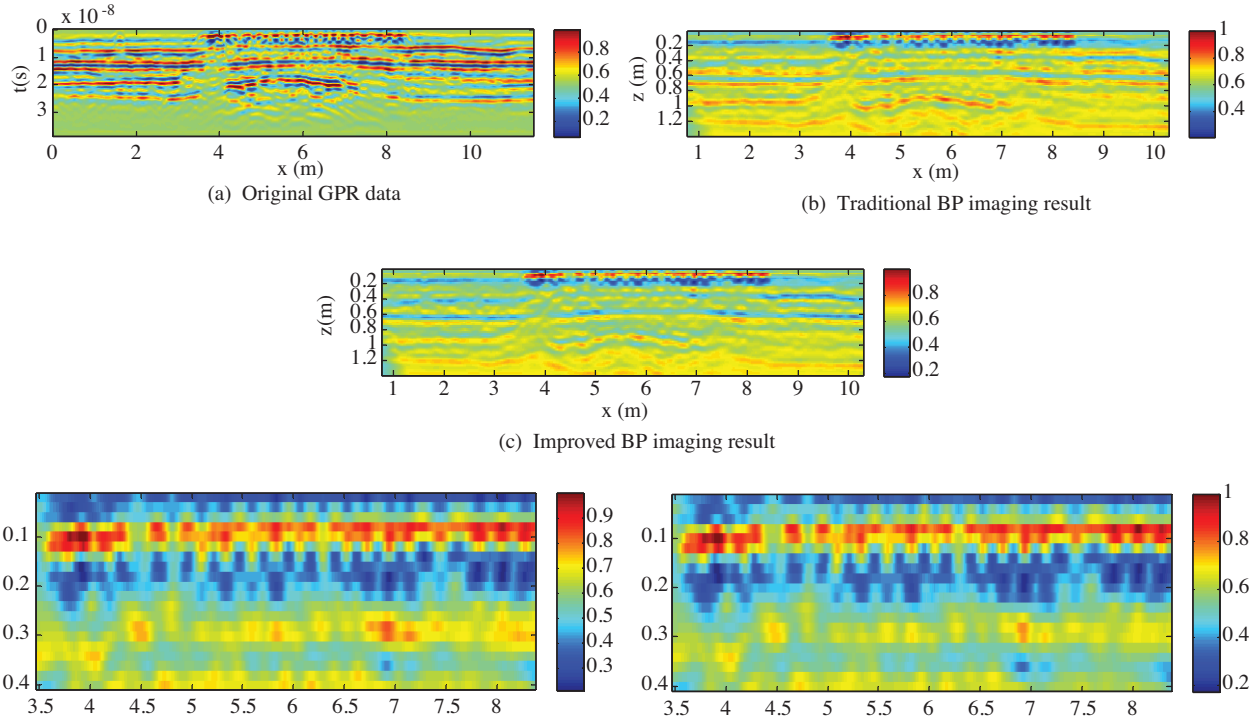


(a) Original GPR data

(b) Traditional BP imaging result

(c) Improved BP imaging result

(d) The contrast between imaging results of steel reinforcement region

**Figure 4.** Real GPR data imaging experiment.

## 4. Summary

An improved BP imaging algorithm is presented in this paper. By analyzing the characteristic of the scattering data at each time-delay curve and by designing a weight factor matrix, the improved imaging algorithm shows a better performance for the aspects of side lobe value and focusing quality. In contrast with the traditional BP imaging algorithm, the computational burden of the improved BP imaging algorithm increased slightly and the quality of the imaging results increased greatly. The simulation results and the real data imaging experiment demonstrated its validity in GPR high resolution imaging. Future work will focus on a fast BP imaging algorithm that is suitable for a subsurface layered medium.

## Acknowledgments

This project was supported by the National Natural Science Foundation of China (No. 61102139), the Research Program of the Ministry of Transport (No. 2011318824350), the Freedom Explore Program of Central South University (No. 2011QNZT024), and the Research Fund of Shanxi Key Laboratory of Electronic Information System Integration (No. 201109Y18).

## References

[1] Y. Su, C. Huang, W. Lei, Theory and Application of Ground Penetrating Radar, Beijing, Science Press, 2006.

[2] H.M. Jol, Ground Penetrating Radar Theory and Applications, the Netherlands, Elsevier Science, 2009.

[3] A.B. Suksmono, E. Bharata, A.A. Lestari, A.G. Yarovoy, L.P. Ligthart, "Compressive stepped-frequency continuous-wave ground-penetrating radar", IEEE Geoscience and Remote Sensing Letters, Vol. 7, pp. 665–669, 2010.

[4] K. Gu, G. Wang, J. Li, "Migration based SAR imaging for ground penetrating radar systems", IEE Proceedings of Radar, Sonar and Navigation, Vol. 151, pp. 317–325, 2004.

[5] W. Lei, L. Liu, C. Huang, Y. Su, "Subsurface imaging of buried objects from FDTD modeled scattered field", Proceedings of the 3rd International Conference on Computational Electromagnetics and Its Applications, pp. 516–520, 2004.

[6] L. Zhou, C. Huang, Y. Su, "A Fast Back-Projection Algorithm Based on Cross Correlation for GPR Imaging", IEEE Geoscience and Remote Sensing Letters, Vol. 9, pp. 228–232, 2012.

[7] D.M. Sullivan, Electromagnetic Simulation Using the FDTD Method, New York, Wiley-IEEE Press, 2000.

[8] H.S. Wu, J. Barba, "Minimum entropy restoration of star field images", IEEE Transactions on Systems, Man and Cybernetics-Part B: Cybernetics, Vol. 28, pp. 227–231, 1998.